Development and Testing of Techniques to Obtain Infiltration Data for Unconsolidated Surficial Materials, Yucca Mountain Area, Nye County, Nevada

By Lon L. Hofmann[1] (Address Unknown), and
William R. Guertal[2] and Alan L. Flint[3], U.S. Geological Survey

[1]Foothill Engineering Consultants, Inc., Denver, Colo. (1995), current affiliation unknown
[2]USGS, Las Vegas, Nev.
[3]USGS, Sacramento, Calif.

U.S. GEOLOGICAL SURVEY

Open-File Report 95–154

Prepared in cooperation with the
U.S. DEPARTMENT OF ENERGY
NEVADA OPERATIONS OFFICE under
Interagency Agreement DE-AI08-97NV12033

Denver, Colorado
2000

U.S. DEPARTMENT OF THE INTERIOR
BRUCE BABBITT, Secretary

U.S. GEOLOGICAL SURVEY
Charles G. Groat, Director

For additional information write to:

Chief, Earth Science Investigations Program
Yucca Mountain Project Branch
U.S. Geological Survey
Box 25046, Mail Stop 421
Denver Federal Center
Denver, CO 80225-0046

Copies of this report can be purchased from:

U.S. Geological Survey
Information Services
Box 25286
Federal Center
Denver, CO 80225

DISCLAIMER

DISCLAIMER

Portions of this document may be illegible in electronic image products. Images are produced from the best available original document.

CONTENTS

FIGURES

TABLES

CONVERSION FACTORS

Multiply	By	To Obtain
centimeter (cm)	0.3937	inch
centimeter per hour (cm/h)	0.7874	feet per day
gram per cubic centimeter (g/cm^3)	62.428	pound per cubic foot
kilometer (km)	0.6214	mile
liter (L)	1.057	quart
meter (m)	3.281	foot
millimeter (mm)	0.03937	inch
millivolt (mV)	0.001	volt
square centimeter (cm^2)	0.001076	square foot

Development and Testing of Techniques to Obtain Infiltration Data for Unconsolidated Surficial Materials, Yucca Mountain Area, Nye County, Nevada

By Lon L. Hofmann, Foothill Engineering Consultants, Inc., (1995) and
William R. Guertal and Alan L. Flint, U.S. Geological Survey

Abstract

Measurements of surface infiltration at Yucca Mountain, Nevada, a potential site for a high-level nuclear-waste repository, are needed to determine spatial variability of hydrologic properties for a wide variety of skeletal desert soils. This report describes and evaluates existing instruments and methods to measure infiltration capacities and their appropriateness for determining hydrologic properties on Yucca Mountain. The report also presents preliminary infiltration data and estimated measurements of saturated hydraulic conductivity and sorptivity and describes the methods used to collect the data.

A prototype automated, constant water-supply-head, double-ring infiltrometer was developed to measure saturated hydraulic conductivity and provide surface-water-flux data to estimate sorptivity. The infiltrometer consisted of an inner confining ring (0.30 to 0.75-meter inside diameter), an outer confining ring (0.6 to 3.5-meter inside diameter), float switches, solenoid valves, a data logger, and water-supply tanks. The prototype automated infiltrometer was used to measure infiltration rates near boreholes UE-25 UZN #85 and UE-25 UZN #14 where large ranges in sorptivity and saturated hydraulic conductivity were expected. The cumulative-infiltration data were fit using the two-term Philip equation from which saturated hydraulic conductivity and sorptivity values were derived. The saturated hydraulic conductivity values at the two sites differed by an order of magnitude. Sorptivity values differed by more than 100 percent between the two sites. Differences in infiltration rates were attributed to differences in measured physical characteristics and differences in initial water contents of soils at the two borehole sites.

INTRODUCTION

The U.S. Geological Survey is conducting investigations to determine the geologic and hydrologic suitability of Yucca Mountain, Nevada, as a potential site for a mined geologic repository for high-level nuclear wastes. These investigations are being conducted in cooperation with the U.S. Department of Energy, under Interagency Agreement DE–AI08–97NV12033, as part of the Yucca Mountain Site Characterization Project (formerly the Nevada Nuclear Waste Storage Investigations Project).

Yucca Mountain consists of a series of ash-flow tuffs that are welded and nonwelded, are variably saturated, and are fractured. Alluvium and other unconsolidated surficial materials overlie most of the tuff (Scott and Castellanos, 1984, p. 7–12). The hydrologic properties of these materials are needed for interpretation of hydrologic data in the unsaturated zone and for input to hydrologic models of Yucca Mountain.

Hydrologic properties, such as saturated hydraulic conductivity (K_s) and sorptivity (S), can be calculated using field-measured flow rates of artificially applied water. Saturated hydraulic conductivity is an important property used in one-dimensional

(1-D) and two-dimensional (2-D) ground-water-flow submodels and in site-scale three-dimensional (3-D) ground-water-flow models (Wittwer and others, 1992, p. 264–265). Field K_s determination involves measuring infiltration rates for an adequate time until an apparent steady-state infiltration rate, which can be interpreted as K_s, is obtained. Sorptivity, a less commonly used property, is a measure of the capillary uptake of water predominating the early time infiltration process. Sorptivity values are dependent on the initial water content (θ_i), the water-retention function [$\theta(\psi)$] where ψ is the water potential, and hydraulic conductivity (K). Sorptivity may be used to determine soil hydraulic properties, such as the hydraulic-conductivity function [$K(\theta)$], and the soil-water-diffusivity function [$D(\theta)$] (Clothier and White, 1981, p. 241–242; White and Perroux, 1987, p. 1094; 1989, p. 324). Sorptivity also has been used in inverse modeling to estimate $K(\theta)$ or [$\theta(\psi)$] (Zimmerman and Bodvarsson, 1989, p. 1423–1426).

Purpose and Scope

This report describes the evaluation of existing instruments and methods to measure infiltration capacities and their appropriateness for measuring hydrologic properties at Yucca Mountain, the performance of a prototype automated infiltrometer, and the quality of the resulting data for estimating field hydrologic properties from selected areas of Yucca Mountain. The report also describes experiments using the prototype automated infiltrometer to obtain preliminary infiltration data and describes the calculated hydrologic parameters of interest, K_s and S, derived from these data.

The scope of the report includes infiltrometer data that were collected from March of 1993 to July of 1993 near two borehole locations drilled in unconsolidated alluvial materials on Yucca Mountain (fig. 1). These sites were chosen because of the likelihood of water ponding on the soil surface and their expected differences in infiltration rates. Infiltration data were collected with a prototype constant-water-supply head, ring infiltrometer (hereinafter referred to as the prototype automated infiltrometer), designed to operate effectively with confining rings of greater than 1-m inside diameter (Hofmann and others, 1993). Because the prototype automated infiltrometer needed to be portable, ring sizes were limited to less than 1-m inside diameter so the double-ring system was used for this study. The infiltration runs were conducted over time periods ranging from 4 to 20 hours. These time periods were adequate to obtain apparent steady-state infiltration rates that were extrapolated as the field-measured K_s value.

Cumulative-infiltration and infiltration-rate curves were developed with the prototype automated infiltrometer for the two borehole locations. The S and A parameters of the Philip equation were fitted to the cumulative-infiltration and infiltration-rate measurements. Comparison of the field-measured K_s to the fitted A parameters was used as a check for the quality of the data.

Definitions and Relations Between Properties

The following section defines the properties that were used to determine infiltration capacity and hydrologic properties at Yucca Mountain. Relations of measured to calculated values also are discussed.

Infiltration

Infiltration is the term applied to the process of water entry into the soil, generally by downward flow through all or part of the soil surface (Hillel, 1980, p. 5).

Cumulative Infiltration

Cumulative infiltration is the summed amount of water that has entered through the soil surface. Cumulative infiltration is calculated as:

$$I = Q/c \qquad (1)$$

where

I = cumulative infiltration, in centimeters;
Q = volume of water entering the soil surface, in liters; and
c = cross-sectional area of soil surface, in centimeters squared.

This value is usually plotted against time to obtain a cumulative-infiltration curve. Fitting of infiltration equations to cumulative-infiltration curves can be used

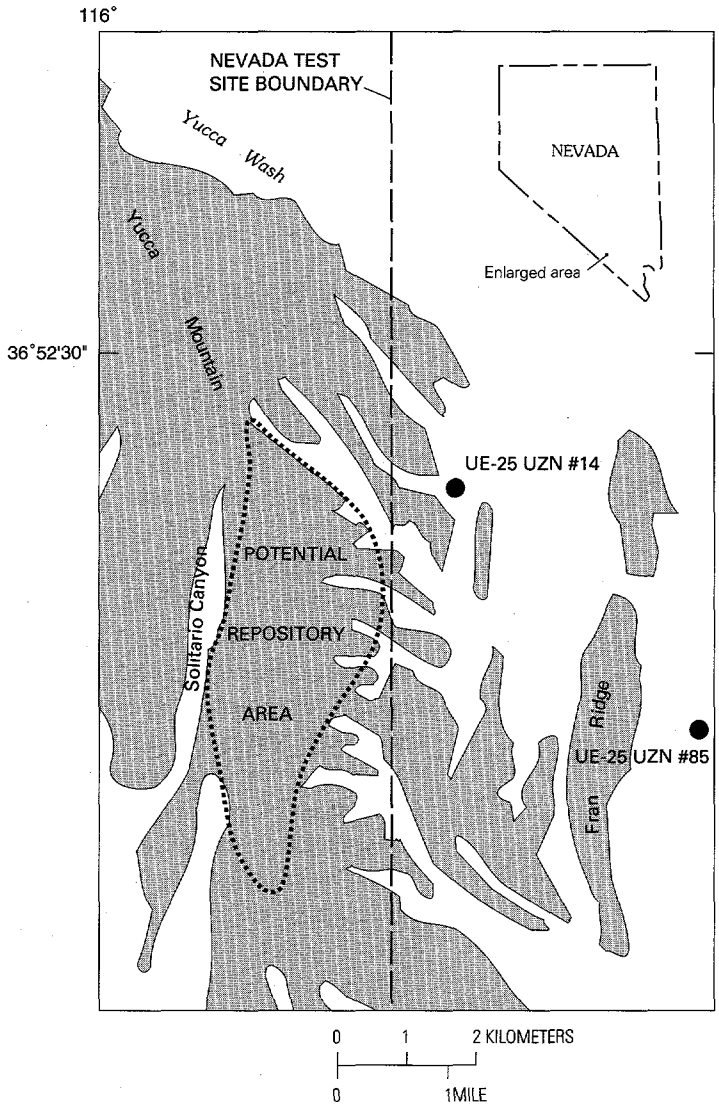

Figure 1. Locations of the automated prototype ring infiltrometer experiments.

to obtain values for hydrologic properties, such as K_s and S.

Infiltration Rate

Infiltration rate is the volume of water flowing into the soil per unit soil surface area (Hillel, 1980, p. 6). Infiltration rate and surface flux are essentially analogous. Infiltration rate is calculated as:

$$i(t) = Q/(ct) \qquad (2)$$

where

(t) = infiltration rate as a function of time, in centimeters per hour.

Sorptivity

Sorptivity describes the rate of uptake of water by a porous medium without gravitational effects (Flint and others, 1994, p. 94). Sorptivity depends on both water-supply-head and initial soil-moisture content. Sorptivity is calculated as:

$$S = I/t^{1/2} \qquad (3)$$

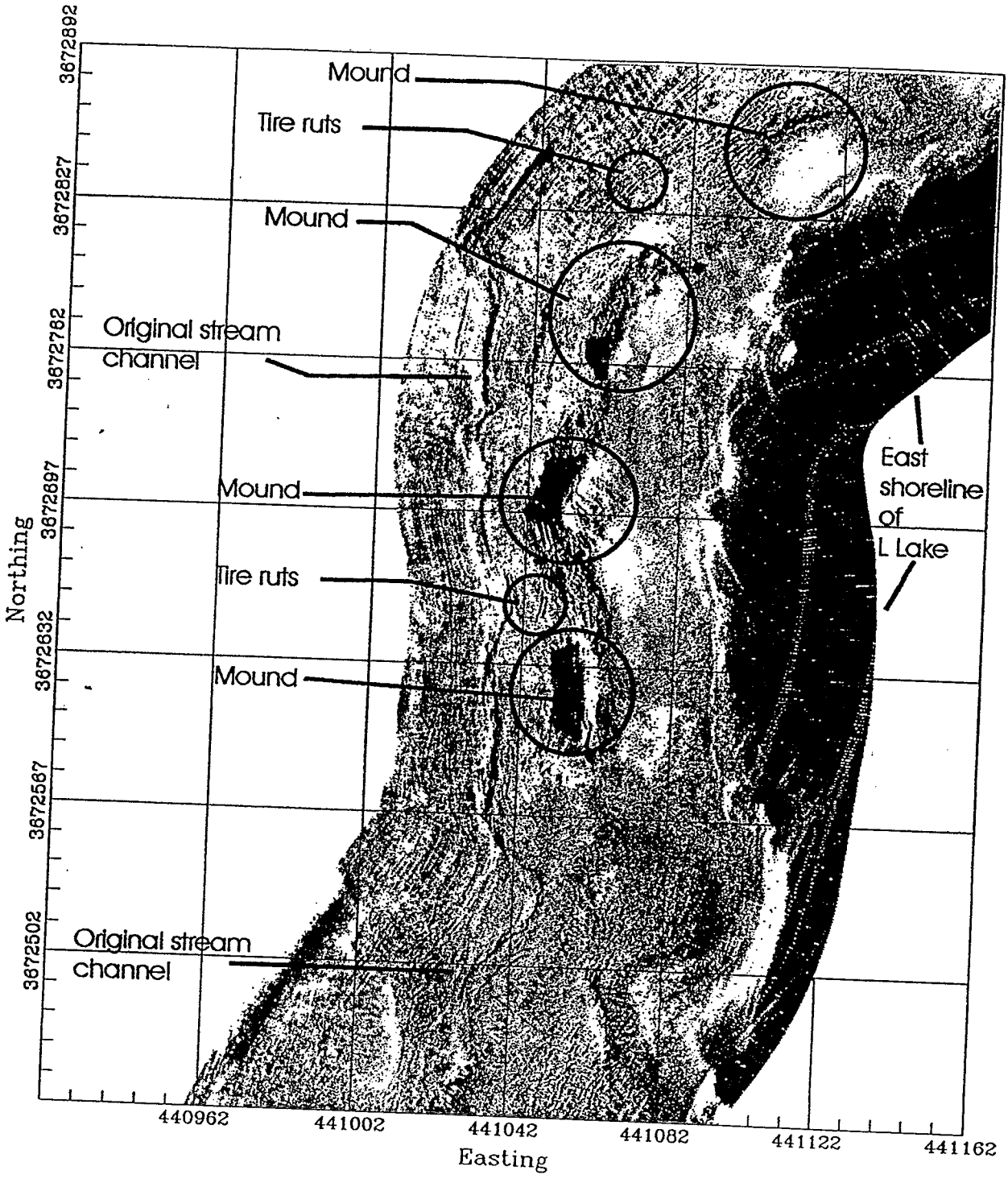

Figure 20. Sonar images of three mounds next to the original stream channel as detected along survey line SL07.

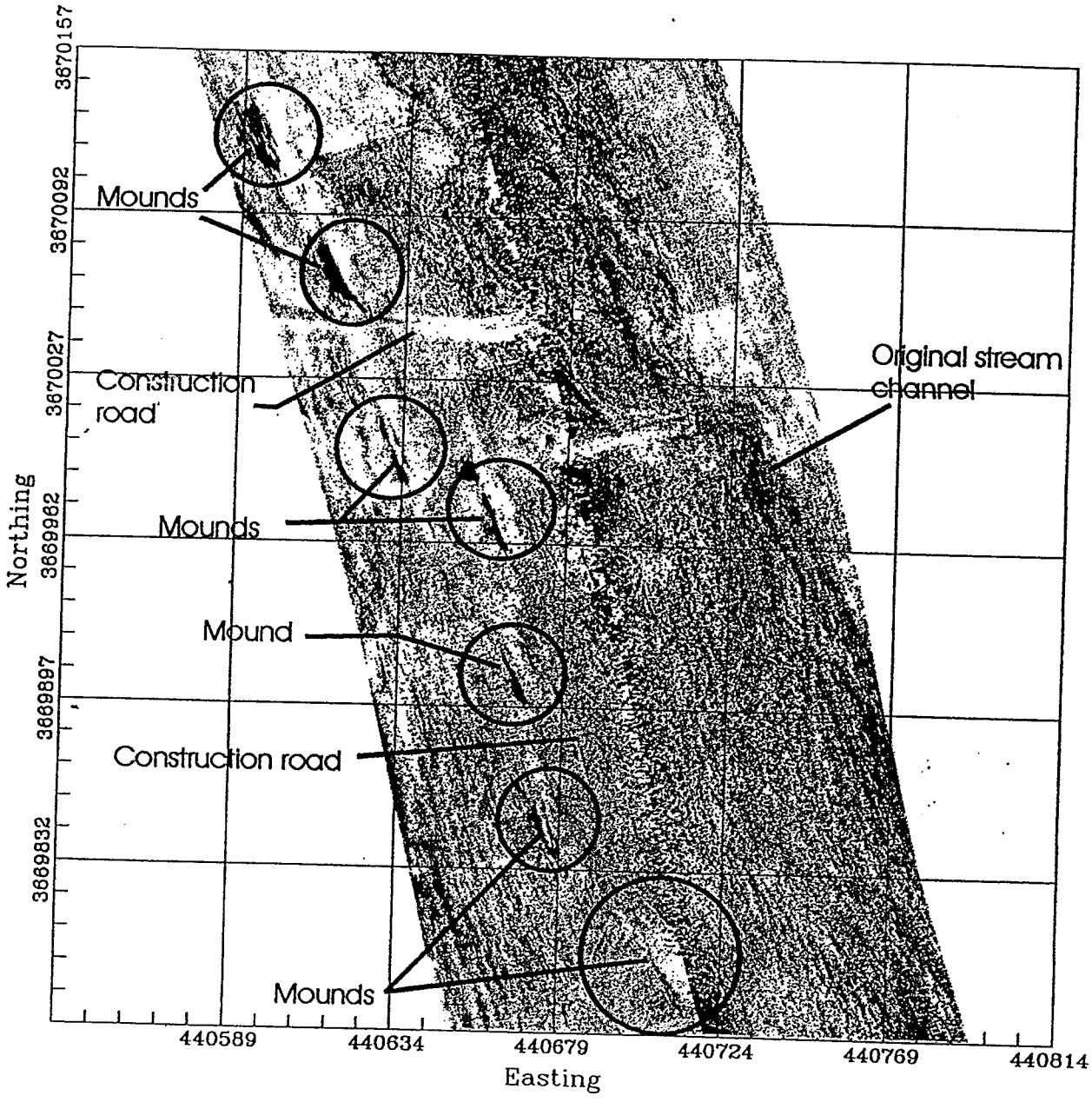

Figure 21. Sonar images of several small mounds along survey line SL03. The original stream channel and construction roads are also detected.

sloping surfaces of Yucca Mountain. A disadvantage of tension infiltrometers is the likelihood of surface disturbances. The permeameter will not function properly if there is not good contact between the membrane-covered disk and the surface of the material. In many places, rock cover would have to be removed or a contact sand layer, our both, would be needed between the membrane-covered disk and the material surface, which could potentially alter the true surface-flow properties. Another disadvantage is that the RESA is limited to the size of the membrane-covered disk, usually around 0.20 m in diameter. Prototype testing is needed to check the adequacy of this tension infiltrometer once it is completed.

Sprinkler-Imposed Steady-Flux Infiltrometer

A sprinkler application of water provides a means of controlling surface flux until a steady-state flow rate in the unconsolidated material is obtained. The K at a selected steady flux is determined by the flux divided by the gradient in hydraulic head over the depth interval of interest (Green and others, 1986, p. 789). Sprinkler application is useful for determining K at soil-water contents close to saturation. Advantages of sprinkler infiltrometers are the flexibility to include various sizes of RESA's. Sprinkler application more closely simulates the physical processes of rainfall infiltration, and the systems can be effectively used on sloping surfaces, which is a major limitation of most other types of infiltrometers.

The major disadvantages of sprinkler infiltrometers are the complexity of their design and the logistics of operating them. First, a plot frame is needed to confine the area of measurement for runoff collection. The runoff collection and measurement is needed for mass-balance calculations. Second, an even water application is needed that, in turn, needs a controlled water-pressure source, which often is inaccessible in the field. This type of infiltrometer should not be used on soils containing layers that are relatively impervious to water flow within the profile which could impede vertical-water flow and thus introduce error in the assumed vertical flux (Green and others, 1986, p. 790).

Advantages of the sprinkler infiltrometer are such that it is practical to use under circumstances that limit the other infiltrometers, but further development and prototype testing of a sprinkler-infiltrometer system that is usable on Yucca Mountain are needed. To obtain an understanding of the range in selected hydrologic properties at Yucca Mountain, an immediate priority was set to develop a much simpler and versatile ring infiltrometer.

Ring Infiltrometer

A ring infiltrometer consists of a circular confining ring in which the water-supply-head is a minimum height of ponded water within the confining ring that is maintained at a constant level. Infiltration measurements are made by measuring the amount of water entering the soil surface in the ring as a function of time (commonly referred to as ponded infiltration). Infiltration measurements using a single large confining ring or smaller double-rings is an approach that can be used to measure cumulative infiltration (Green and others, 1986, p. 791–793). Ponded areas larger than 1.2 m would maximize the likelihood of 1-D flow measurements using a single confining ring (Bouwer, 1986, p. 830–831). Double-ring infiltrometers, where a larger ring is placed around a smaller ring concentrically, have been used to limit lateral divergence of water infiltrating in the inner ring that has an inside diameter less than 1.2 m. Cumulative-infiltration and infiltration-rate measurements are used to calculate K_s and S (Young, 1968, p. 159–160; Talsma, 1969, p. 270–275; Talsma and Parlange, 1972, p. 146–149; Green and others, 1986, p. 791–793).

The ring infiltrometer is one of the most versatile types of infiltrometers that can be used for measuring hydrologic properties under ponded conditions. Infiltrometer ring sizes can be adjusted to include practically any size RESA. Most double-ring infiltrometers are relatively portable. A disadvantage of ring infiltrometers is that some degree of surface disturbance is likely when placing the rings into the ground, especially in skeletal materials. Double-ring-infiltrometer ponding studies also are limited to areas with less than 3 percent slope. Differences in ponded-head height across the surface area of the infiltrometer rings on sloping surfaces greater than 3 percent could induce deviations from 1-D vertical flow.

An already developed ring infiltrometer was easily automated and was made capable of measuring infiltration rates with a high degree of accuracy. The prototype automated infiltrometer consists of an inner and outer ring, magnetic-reed switch-float sensors,

solenoid valves, data logger, and water-supply tanks (fig. 2). Mechanical operation of the infiltrometer is the same despite the size of the confining ring. The depth of water-supply head is maintained by two magnetic-reed switch-float sensors. When the water-supply-head level reaches a minimum height, one of the float sensors sends a pulse signal to a data logger that opens an electronic solenoid valve, allowing water to flow into the confining infiltrometer ring, by gravity, from the supply tank. Once the water-supply head reaches a preset maximum depth, the other float sensor sends a pulse to the data logger that closes the solenoid valve. Ten seconds after the solenoid valve shuts off, the data logger reads and records the pressure transducer output along with the corresponding time. It is these time readings that are used to calculate infiltration rates. These time intervals range from 0 to 30 minutes depending on the infiltration rates.

Water is supplied to each ring individually by a cylindrical 210-L tank fitted with a pressure transducer that has been calibrated to measure cumulative water outflow. Calibration of the pressure transducer with the water-supply tank involves release of water from the supply tank at known volumes. For each incremental release of water from the supply tank, a corresponding pressure-transducer reading is made. This pressure-transducer reading represents the change in supply-tank water height because a known volume of water has been released. This calibration also accounts for physical changes in supply-tank dimensions.

The pressure transducer is calibrated to the water-supply tank using a least-squares equation:

$$PT = a + b(q) \tag{6}$$

where

PT = the pressure-transducer reading, in millivolts;
a = the initial pressure transducer reading before release of water from the supply tank; that is, when q = 0;
b = the least-squares slope relation of supply-tank volume-outflow change per change in pressure transducer reading; and
q = cumulative volume water outflow from the supply-tank, in liters.

The calibration equation is rearranged to calculate cumulative volume of water flow into the prototype automated infiltrometer confining rings, in liters:

$$q = (PT - a)/b \tag{7}$$

Dividing the cumulative volume outflow of water by the surface area of the confining ring results in cumulative infiltration:

$$I = q/c \tag{8}$$

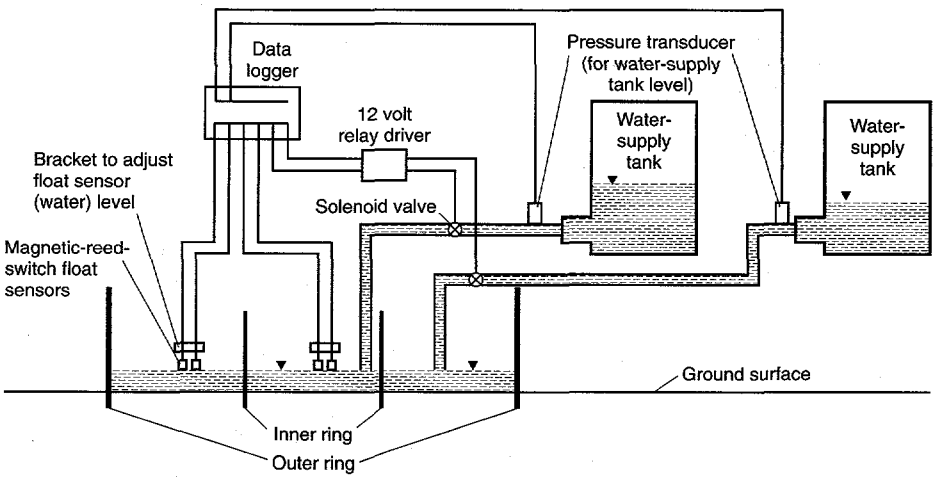

Figure 2. Automated prototype constant-water-supply head, ring infiltrometers.

where

I = cumulative infiltration, in centimeters; and

c = the cross-sectional area of the soil surface, in centimeters squared.

To obtain the infiltration rate, cumulative infiltration is divided by the time step at which the pressure transducer was read. Thus, infiltration rate is calculated by:

$$i = I/t \tag{9}$$

where

i = infiltration rate, in centimeters per unit time; and

t = time, in hours.

EXPERIMENTAL RESULTS

Locations and Procedures

The prototype automated infiltrometer was installed in two locations at Yucca Mountain: in Pagany Wash near borehole UE-25 UZN #14 (N14), and on a stable terrace adjacent to Fortymile Wash at borehole UE-25 UZN #85 (N85) (fig. 1). A small-scale version of the prototype automated infiltrometer was used near N14, consisting of an inner confining ring that had a 0.30-m inside diameter surrounded by an outer ring that had a 0.64-m inside diameter. A large-scale version was used at N85 consisting of an outer ring that had a 3.5-m inside diameter and three inner rings having 0.75-m inside diameters that were spaced 1 m apart. The inner rings of the large-scale infiltrometer were considered to be independent replications of the ponded-infiltration experiment. Surface slope was less than 3 percent at both locations. The bottom edge of the confining ring was implanted below the soil surface at a minimum depth of 0.15 m to ensure 1-D vertical flow of infiltrating water.

Cumulative-infiltration and infiltration-rate curves were developed from the data obtained with both types of prototype automated infiltrometers using equations 7, 8, and 9. Equations 4 and 5 were fit to the developed infiltration curves by means of the least-squares technique to obtain values for the S and A parameters. Measured K_s values were compared to 30 to 60 percent of parameter A. The parameters of equations 4 and 5 are physically based; therefore, differences in experimental results would be expected to be related to physical properties, such as pore-size distribution and porosity. Bulk density and porosity of representative samples collected in the area of the two boreholes were measured.

Operation of Prototype Automated Infiltrometer

Water-supply-tank calibration data are listed in table 1. Least-squares linear regression calibration equations, derived from the data presented in table 1, for the prototype automated infiltrometers are listed in table 2. The calibration equations in table 2 are based on equation 6. Water-supply-tank-measurement accuracies ranged from 0.083 to 0.131 L at one standard deviation between the three supply tanks used. For an infiltrometer ring that had a 1-m inside diameter, this range in calibration variability would result in an error of 0.03 to 0.05 cm of infiltrated water at an $\alpha = 0.025$, where $(1-\alpha)$ is the confidence coefficient.

The prototype automated infiltrometer performed well with minimal man-hour input. A constant depth of ponded water was maintained over the soil surface at a minimum ponding depth of 1.0 cm, 0.1 cm during the infiltration experiments. Once the prototype automated infiltrometer was operating, refilling the water-supply tank and data collection from the data logger were the only requirements to conduct the experiments.

Infiltration-Capacity Measurements

Cumulative-infiltration curves were successfully constructed for both sampling washes at Yucca Mountain using data from the prototype automated infiltrometer and equation 8. Cumulative-infiltration rates (fig. 3) measured by two of the three inner confining rings were similar at the N85 location. Data used to construct the curves in figure 3 are listed in table 3. Reliable data from the third inner ring could not be collected because the pressure transducer for the water-supply tank failed; only results from the two inner rings are presented in figure 3 and table 3. Early-time infiltration was very similar for both rings, but the

Table 1. Volumetric water outflow and pressure transducer calibration data from the prototype-automated-infiltrometer water-supply tank

[All cumulative volume-outflow measurements in liters; all pressure-transducer readings in millivolts]

Tank 1		Tank 2		Tank 3	
Cumulative volume outflow	Pressure outflow reading	Cumulative volume outflow	Pressure outflow reading	Cumulative volume outflow	Pressure outflow reading
0.0	-0.501	0.0	-0.414	0.0	0.690
2.0	-0.503	2.0	-0.415	2.0	0.688
4.0	-0.504	4.0	-0.417	4.1	0.687
6.0	-0.506	6.0	-0.418	6.1	0.685
8.0	-0.508	8.0	-0.420	8.1	0.683
10.0	-0.509	10.1	-0.421	10.1	0.681
12.0	-0.511	12.1	-0.423	12.1	0.679
14.0	-0.513	14.0	-0.425	14.1	0.678
16.0	-0.515	16.0	-0.427	16.1	0.676
18.0	-0.516	18.0	-0.428	18.2	0.673
20.0	-0.518	20.0	-0.430	20.2	0.672
22.0	-0.520	22.1	-0.432	22.2	0.670
24.0	-0.522	24.1	-0.434	24.2	0.668
26.1	-0.523	26.1	-0.435	26.2	0.666
28.1	-0.525	28.1	-0.437	28.2	0.664
30.1	-0.527	30.0	-0.439	30.2	0.662
32.1	-0.529	32.1	-0.440	32.2	0.660
34.1	-0.530	34.1	-0.442	34.3	0.658
36.1	-0.532	36.1	-0.444	36.3	0.656
38.1	-0.534	38.1	-0.445	38.3	0.655
40.1	-0.536	40.1	-0.447	40.3	0.653
42.1	-0.537	42.1	-0.448	42.3	0.651
44.1	-0.539	44.1	-0.450	44.3	0.649
46.1	-0.541	46.1	-0.452	46.3	0.647
48.1	-0.543	48.1	-0.453	48.3	0.645
50.1	-0.544	50.1	-0.455	50.3	0.643
52.1	-0.546	52.1	-0.457	52.3	0.641
54.1	-0.548	54.1	-0.459	54.3	0.639
56.1	-0.550	56.1	-0.460	56.4	0.638
58.1	-0.551	58.1	-0.462	58.4	0.636
60.1	-0.553	60.1	-0.464	60.4	0.634
62.1	-0.555	62.1	-0.465	62.4	0.632
64.1	-0.557	64.1	-0.467	64.4	0.630
66.2	-0.558	66.1	-0.469	66.4	0.628
68.2	-0.560	68.1	-0.470	68.4	0.627

Table 1. Volumetric water outflow and pressure transducer calibration data from the prototype-automated-infiltrometer water-supply tank—Continued

[All cumulative volume-outflow measurements in liters; all pressure-transducer readings in millivolts]

Tank 1		Tank 2		Tank 3	
Cumulative volume outflow	Pressure outflow reading	Cumulative volume outflow	Pressure outflow reading	Cumulative volume outflow	Pressure outflow reading
70.2	-0.562	70.1	-0.472	70.4	0.625
72.2	-0.564	72.1	-0.474	72.4	0.623
74.2	-0.566	74.1	-0.475	74.4	0.621
76.2	-0.567	76.1	-0.477	76.4	0.619
78.2	-0.569	78.1	-0.479	78.4	0.617
80.2	-0.571	80.1	-0.480	80.5	0.615
82.2	-0.573	82.1	-0.482	82.4	0.613
84.3	-0.574	84.1	-0.484	84.4	0.612
86.3	-0.576	86.2	-0.485	86.4	0.610
88.3	-0.578	88.2	-0.487	88.4	0.608
90.3	-0.580	90.2	-0.489	90.4	0.606
92.3	-0.581	92.2	-0.490	92.5	0.604
94.2	-0.583	94.2	-0.492	94.5	0.602
96.3	-0.585	96.2	-0.494	96.5	0.601
98.3	-0.587	98.2	-0.495	98.5	0.599
100.3	-0.588	100.3	-0.497	100.5	0.597
102.3	-0.590	102.3	-0.499	102.5	0.595
104.3	-0.592	104.3	-0.501	104.5	0.593
106.3	-0.594	106.3	-0.502	106.5	0.591
108.3	-0.595	108.2	-0.504	108.5	0.589
110.3	-0.597	110.2	-0.506	110.6	0.588
112.3	-0.599	112.2	-0.507	112.6	0.586
114.3	-0.601	114.3	-0.509	114.6	0.584
116.3	-0.603	116.3	-0.511	116.6	0.582
118.3	-0.604	118.3	-0.512	118.6	0.580
120.3	-0.606	120.3	-0.514	120.6	0.578
122.3	-0.608	122.3	-0.516	122.6	0.576
124.3	-0.610	124.3	-0.517	124.6	0.575
126.3	-0.611	126.3	-0.519	126.6	0.573
128.4	-0.613	128.3	-0.521	128.6	0.571
130.4	-0.615	130.3	-0.522	130.6	0.569
132.4	-0.617	132.3	-0.524	132.5	0.567
134.4	-0.618	134.3	-0.526	134.6	0.565
136.4	-0.620	136.3	-0.527	136.5	0.564
138.4	-0.622	138.3	-0.529	138.6	0.562
140.4	-0.624	140.3	-0.531	140.6	0.560

Table 1. Volumetric water outflow and pressure transducer calibration data from the prototype-automated-infiltrometer water-supply tank—Continued

[All cumulative volume-outflow measurements in liters; all pressure-transducer readings in millivolts]

Tank 1		Tank 2		Tank 3	
Cumulative volume outflow	Pressure outflow reading	Cumulative volume outflow	Pressure outflow reading	Cumulative volume outflow	Pressure outflow reading
142.4	-0.625	142.3	-0.532	142.6	0.558
144.4	-0.627	144.3	-0.534	144.6	0.556
146.4	-0.629	146.3	-0.536	146.6	0.554
148.4	-0.631	148.4	-0.538	148.6	0.552
150.4	-0.632	150.4	-0.539	150.6	0.551
152.4	-0.634	152.4	-0.541	152.6	0.549
154.4	-0.636	154.4	-0.543	154.6	0.547
156.4	-0.638	156.4	-0.544	156.6	0.545
158.4	-0.639	158.4	-0.546	158.6	0.543
160.4	-0.641	160.4	-0.548	160.6	0.541
162.4	-0.643	162.4	-0.549	162.6	0.540
164.4	-0.645	164.4	-0.551	164.6	0.538
166.4	-0.646	166.4	-0.553	166.6	0.536
168.4	-0.648	168.4	-0.554	168.7	0.534
170.4	-0.650	170.4	-0.556	170.7	0.532
172.4	-0.652	172.5	-0.558	172.7	0.530
174.4	-0.653	174.5	-0.559	174.7	0.529
176.4	-0.655	176.5	-0.561		
178.4	-0.657	178.5	-0.562		
		180.5	-0.564		

Table 2. Least-squares linear-regression equations for calibrating data from the water-supply tank and the pressure transducer of the prototype automated infiltrometer (data are in table 1)

[The x regression variable is supply-tank cumulative-volume outflow and the y regression variable is pressure-transducer reading]

Tank	Least-squares linear-regression equation	Coefficient of determination r^2	Standard error of estimate (millivolts)
1	y = -0.50065 - 0.00088(x)	1.000	0.00007
2	y = -0.41331 - 0.00084(x)	1.000	0.00011
3	y = 0.69012 - 0.00093(x)	1.000	0.00026

curves began to diverge after about 5 hours of infiltration. Sorptivity predominates early-time infiltration processes, whereas gravity gradually becomes the predominating force as the depth of the infiltrating wetting front increases. Spatial variability in subsurface restrictive layers to water flow could account for the divergence between the infiltration curves during the long-term infiltration process. These results support the assumption that the *S* values between the two rings were similar, whereas greater variability occurred between the *A* parameters.

A cumulative-infiltration curve (fig. 4) was constructed using data (table 3) obtained from the small-scale infiltrometer in Pagany Wash near borehole N14. Infiltration rates were larger near the N14 location than at the N85 location (table 3). Eighty centimeters of water had infiltrated near N14 after 4 hours compared to 10 cm of water at the N85 location (figs. 3 and 4). Evaporation losses from infiltrating water were a concern during the experiments, but maximum potential infiltration losses did not exceed 0.5 cm at either location for the duration of the infiltration runs, which accounted for less than 1 percent of the total infiltrated water.

The least-squares technique was used to fit the Philip equation to the cumulative-infiltration data from the two infiltrometer rings at the N85 location (fig. 3) and to the data from the N14 location (fig. 4). Sorptivity values for the two infiltrometer rings at the N85 location varied by less than 1 cm/h$^{1/2}$, whereas the *A* parameter varied by less than 0.6 cm/h (table 4). The divergence of the cumulative-infiltration curves observed in the data (fig. 3) is reflected by the different values of *S* and *A*. At N14, the *S* and *A* parameters were considerably different from those obtained at N85 (table 4).

Saturated hydraulic conductivity values extrapolated from the infiltration-rate curves between the two

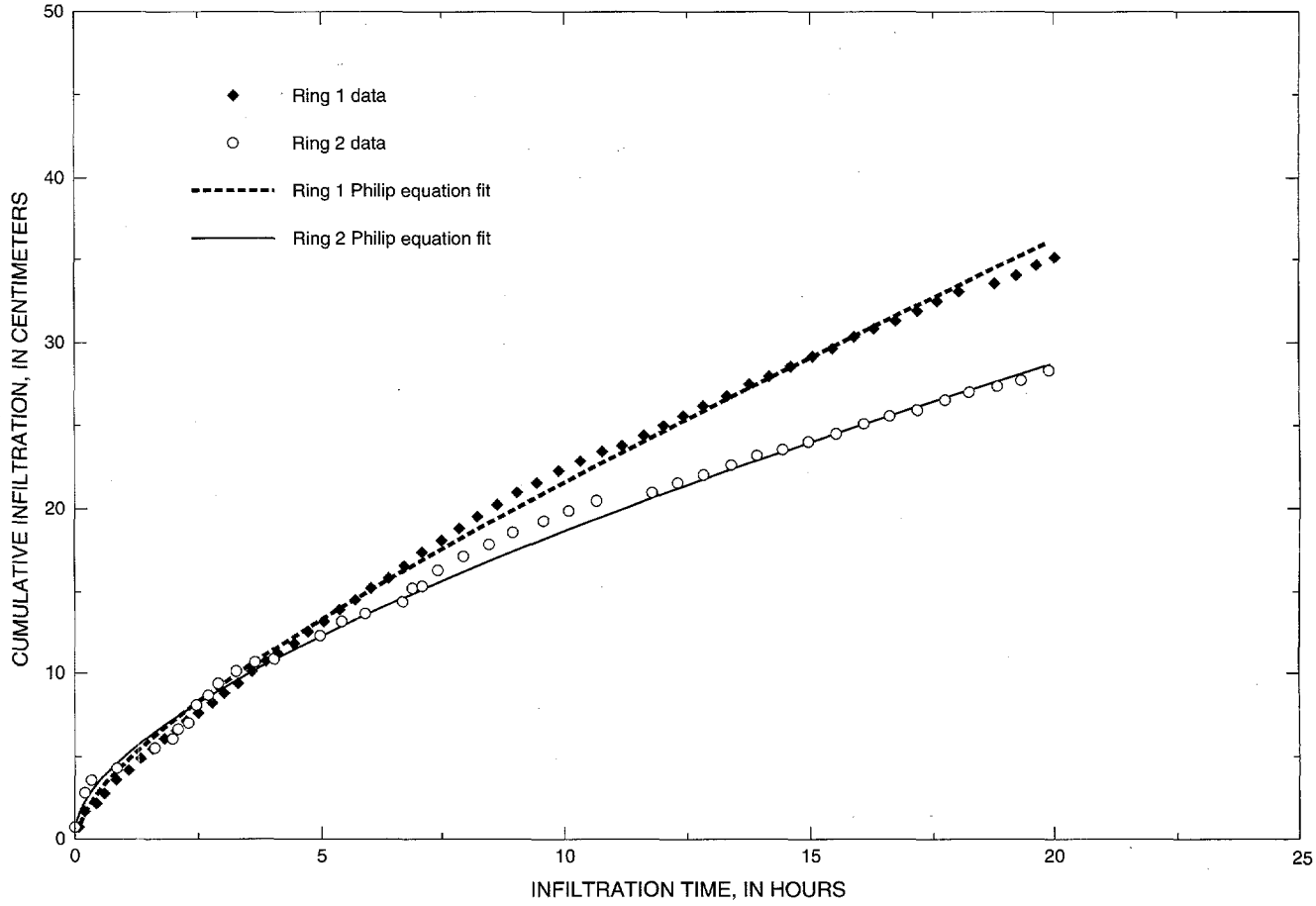

Figure 3. Cumulative-infiltration data and Philip-equation fit obtained near borehole UE-25 UZN #85, Yucca Mountain, Nevada.

Table 3. Cumulative-infiltration and infiltration-rate data using the automated prototype infiltrometer

Ring location	Infiltration time (hours)	Cumulative infiltration (centimeters)	Infiltration rate (centimeters per hour)
UE-25 UZN #85	0.07	0.7	10.1
Ring 1	0.19	1.7	8.8
	0.46	2.1	4.6
	0.60	2.7	4.5
	0.84	3.6	4.3
	1.09	4.2	3.9
	1.34	4.9	3.6
	1.58	5.5	3.5
	1.82	6.1	3.3
	2.08	6.6	3.2
	2.28	7.1	3.1
	2.52	7.6	3.0
	2.77	8.3	3.0
	3.04	8.9	2.9
	3.32	9.5	2.9
	3.59	10.1	2.8
	3.88	10.7	2.8
	4.13	11.3	2.7
	4.44	11.8	2.7
	4.74	12.5	2.6
	5.05	13.2	2.6
	5.37	13.9	2.6
	5.70	14.5	2.5
	6.04	15.2	2.5
	6.38	15.8	2.5
UE-25 UZN #85	6.73	16.5	2.5
Ring 1	7.09	17.3	2.4
	7.46	18.0	2.4
	7.84	18.8	2.4
	8.21	19.6	2.4
	8.62	20.2	2.3
	9.01	20.9	2.3
	9.44	21.6	2.3
	9.86	22.2	2.3
	10.32	22.8	2.2
	10.75	23.4	2.2
	11.17	23.8	2.1
	11.60	24.4	2.1
	12.00	25.0	2.1
	12.41	25.6	2.1
	12.84	26.2	2.0
	13.30	26.9	2.0
	13.76	27.5	2.0
	14.16	28.0	2.0
	14.60	28.6	2.0
	15.05	29.2	1.9
	15.46	29.7	1.9

Table 3. Cumulative-infiltration and infiltration-rate data using the automated prototype infiltrometer—Continued

Ring location	Infiltration time (hours)	Cumulative infiltration (centimeters)	Infiltration rate (centimeters per hour)
	15.90	30.3	1.9
	16.32	30.9	1.9
	16.75	31.4	1.9
	17.19	31.9	1.9
	17.61	32.5	1.8
	18.04	33.1	1.8
UE-25 UZN #85	18.79	33.6	1.8
Ring 1	19.21	34.1	1.8
	19.64	34.7	1.8
	20.00	35.1	1.8
UE-25 UZN #85	0.05	0.6	12.3
Ring 2	0.12	1.9	16.5
	0.24	2.8	11.7
	0.39	3.5	8.9
	0.88	4.1	4.7
	1.65	5.4	3.3
	2.04	6.0	3.0
	2.16	6.5	3.0
	2.33	7.0	3.0
	2.50	8.0	3.2
	2.74	8.6	3.1
	2.97	9.3	3.1
	3.31	10.1	3.0
	3.69	10.6	2.9
	4.10	10.8	2.6
	5.01	12.2	2.4
	5.46	13.0	2.4
	5.95	13.6	2.3
	6.70	14.2	2.1
	6.92	15.0	2.2
	7.12	15.2	2.1
	7.43	16.1	2.2
	7.95	17.0	2.1
UE-25 UZN #85	8.48	17.7	2.1
Ring 2	8.99	18.4	2.1
	9.59	19.1	2.0
	10.13	19.7	1.9
	10.69	20.3	1.9
	11.81	20.9	1.8
	12.34	21.4	1.7
	12.85	21.9	1.7
	13.41	22.5	1.7
	13.94	23.0	1.7
	14.46	23.5	1.6
	15.03	23.9	1.6

Table 3. Cumulative-infiltration and infiltration-rate data using the automated prototype infiltrometer—Continued

Ring location	Infiltration time (hours)	Cumulative infiltration (centimeters)	Infiltration rate (centimeters per hour)
	15.57	24.4	1.6
	16.13	25.0	1.5
	16.68	25.5	1.5
	17.22	25.9	1.5
	17.81	26.4	1.5
	18.27	26.9	1.5
	18.85	27.2	1.4
	19.34	27.6	1.4
	19.90	28.2	1.4
UE-25 UZN #14	0.0	0.0	0.0
	0.03	2.3	67.9
	0.05	2.8	56.6
	0.07	3.4	51.4
	0.10	4.7	47.1
	0.12	4.8	41.4
UE-25 UZN #14	0.13	5.2	39.0
	0.15	6.2	41.2
	0.17	8.2	49.2
	0.20	8.7	43.3
	0.22	7.8	35.8
	0.25	8.1	32.3
	0.27	9.0	33.7
	0.28	9.4	33.3
	0.32	9.2	29.1
	0.33	10.0	30.1
	0.35	10.2	29.2
	0.38	12.0	31.2
	0.40	13.1	32.7
	0.42	12.1	29.1
	0.45	12.1	26.8
	0.47	11.0	23.5
	0.48	12.9	26.7
	0.52	13.1	25.4
	0.53	14.2	26.7
	0.57	14.5	25.6
	0.58	15.2	26.0
	0.60	14.8	24.6
	0.63	12.3	19.4
	0.65	12.0	18.5
	0.68	15.5	22.7
	0.70	17.7	25.3
	0.72	18.6	26.0
	0.75	20.7	27.6
UE-25 UZN #14	0.77	21.0	27.3
	0.80	20.7	25.8

Table 3. Cumulative-infiltration and infiltration-rate data using the automated prototype infiltrometer—Continued

Ring location	Infiltration time (hours)	Cumulative infiltration (centimeters)	Infiltration rate (centimeters per hour)
	0.82	20.1	24.7
	0.85	21.4	25.1
	0.87	21.2	24.4
	0.88	20.0	22.6
	0.92	19.6	21.4
	0.93	20.8	22.3
	0.97	22.0	22.7
	0.98	23.2	23.6
	1.00	22.7	22.7
	1.03	23.5	22.8
	1.05	21.9	20.8
	1.07	21.8	20.4
	1.10	22.1	20.1
	1.12	22.3	20.0
	1.13	23.5	20.7
	1.17	23.5	20.2
	1.18	24.6	20.7
	1.20	25.2	21.0
	1.23	26.0	21.1
	1.25	26.9	21.5
	1.27	27.5	21.7
	1.30	26.6	20.4
	1.32	26.5	20.1
	1.33	26.9	20.2
	1.37	28.2	20.6
	1.38	28.9	20.9
UE-25 UZN #14	1.40	28.5	20.4
	1.42	28.5	20.1
	1.45	28.9	19.9
	1.47	28.3	19.3
	1.48	28.4	19.1
	1.50	30.9	20.6
	1.53	32.8	21.4
	1.55	34.5	22.2
	1.57	33.5	21.4
	1.60	34.5	21.6
	1.62	33.3	20.6
	1.63	33.3	20.3
	1.67	34.8	20.9
	1.68	33.3	19.8
	1.72	34.1	19.9
	1.73	35.0	20.2
	1.77	35.6	20.1
	1.78	36.4	20.4
	1.82	34.7	19.1
	1.83	35.9	19.6

Table 3. Cumulative-infiltration and infiltration-rate data using the automated prototype infiltrometer—Continued

Ring location	Infiltration time (hours)	Cumulative infiltration (centimeters)	Infiltration rate (centimeters per hour)
	1.87	36.5	19.5
	1.88	37.6	20.0
	1.92	38.4	20.0
	1.93	37.6	19.4
	1.97	38.9	19.8
	2.00	39.4	19.7
	2.02	39.8	19.7
	2.05	40.5	19.8
UE-25 UZN #14	2.08	40.1	19.3
	2.10	40.9	19.5
	2.13	42.1	19.7
	2.15	42.0	19.5
	2.18	42.2	19.3
	2.20	43.0	19.5
	2.23	42.7	19.1
	2.27	42.3	18.6
	2.28	41.7	18.3
	2.32	42.1	18.2
	2.33	42.9	18.4
	2.37	45.7	19.3
	2.38	47.1	19.8
	2.42	46.0	19.0
	2.43	45.5	18.7
	2.47	46.5	18.9
	2.48	48.2	19.4
	2.52	49.2	19.5
	2.55	49.2	19.3
	2.57	49.9	19.4
	2.60	49.9	19.2
	2.62	49.8	19.0
	2.65	51.2	19.3
	2.67	50.3	18.9
	2.70	51.6	19.1
	2.72	51.1	18.8
	2.75	51.3	18.6
	2.77	50.7	18.3
UE-25 UZN #14	2.80	52.3	18.7
	2.82	52.6	18.7
	2.85	53.5	18.8
	2.87	54.6	19.0
	2.90	53.5	18.4
	2.92	52.1	17.9
	2.95	53.3	18.1
	2.97	53.7	18.1
	3.00	53.8	17.9
	3.02	55.9	18.5

Table 3. Cumulative-infiltration and infiltration-rate data using the automated prototype infiltrometer—Continued

Ring location	Infiltration time (hours)	Cumulative infiltration (centimeters)	Infiltration rate (centimeters per hour)
	3.05	56.8	18.6
	3.07	55.7	18.1
	3.10	54.8	17.7
	3.12	55.4	17.8
	3.15	56.4	17.9
	3.18	56.7	17.8
	3.20	57.6	18.0
	3.23	58.4	18.0
	3.25	57.3	17.6
	3.28	58.4	17.8
	3.30	59.2	17.9
	3.33	60.7	18.2
	3.37	60.3	17.9
	3.38	60.9	18.0
	3.42	60.7	17.8
	3.43	60.0	17.5
	3.47	62.2	17.9
	3.48	62.6	18
UE-25 UZN #14	3.52	62.8	17.9
	3.53	62.8	17.8
	3.57	63.9	17.9
	3.58	63.2	17.6
	3.62	65.1	18.0
	3.63	65.6	18.1
	3.67	65.6	17.9
	3.68	64.9	17.6
	3.70	64.4	17.4
	3.73	64.7	17.3
	3.75	64.9	17.3
	3.78	67.3	17.8
	3.80	67.9	17.9
	3.82	66.8	17.5
	3.85	67.0	17.4
	3.87	67.5	17.4
	3.90	69.2	17.7
	3.92	69.7	17.8
	3.95	70.1	17.7
	3.97	70.5	17.8
	3.98	71.7	18.0

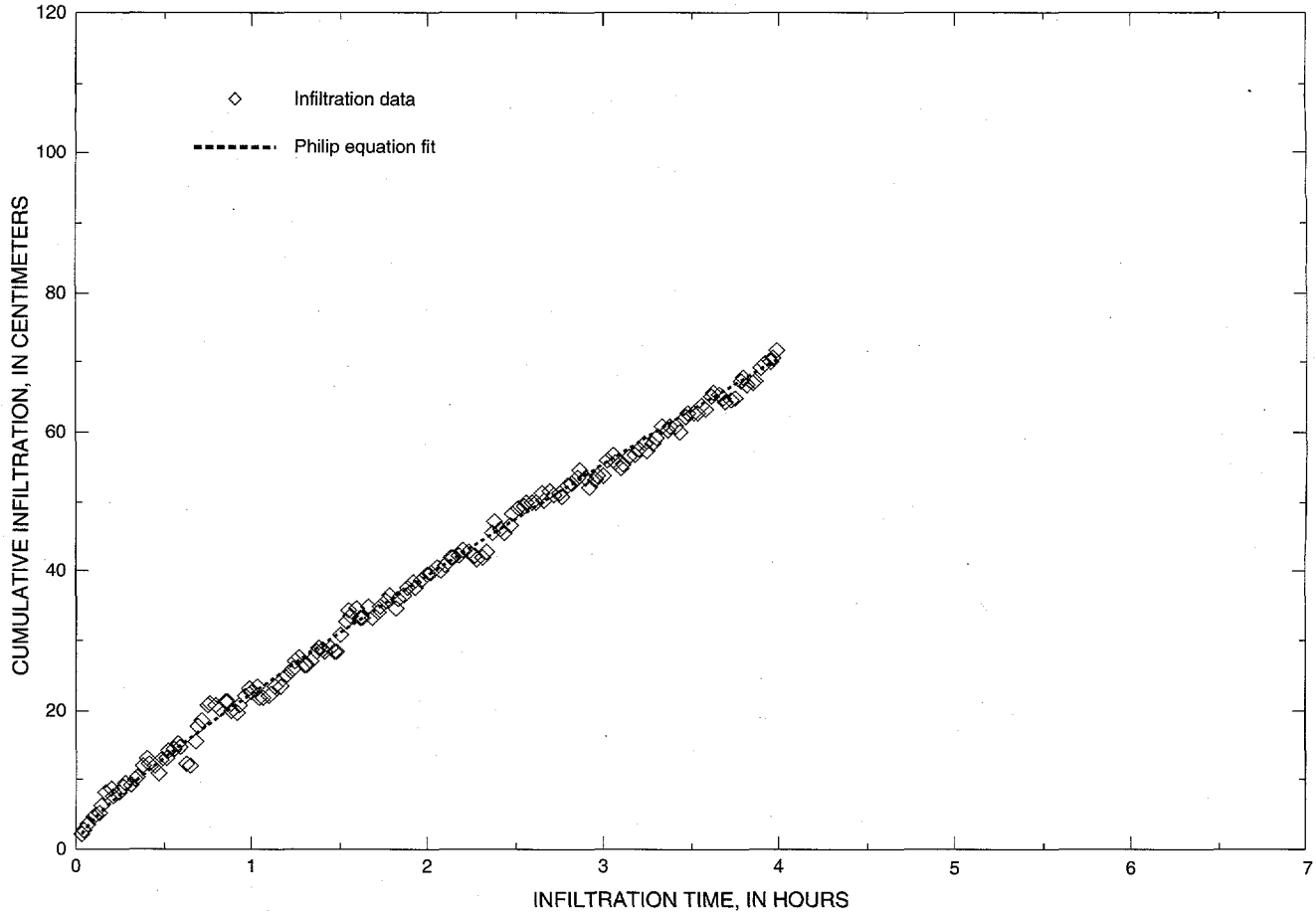

Figure 4. Cumulative-infiltration data and Philip-equation fit obtained near borehole UE-25 UZN #14, Yucca Mountain, Nevada.

experiment sites differed by an order of magnitude (table 4). These differences in K_s can be attributed to the different physical characteristics of the unconsolidated materials. Bulk densities of unconsolidated material averaged 1.89 g/cm^3 in the area of N85, whereas bulk densities averaged 1.41 g/cm^3 in the area of N14. Particle densities of unconsolidated materials on Yucca Mountain were fairly uniform; the measured average values were 2.54 g/cm^3. The differences in bulk densities between the two sites resulted in total porosities of 0.26 in the area of N85 and 0.44 in the area of N14. The larger porosities in the area of N14, in combination with little or no cementing of subsurface materials, may account for the differences in calculated hydraulic properties at the two sites. Differences in clay content (16 percent in the area of N85 compared to less than 4 percent in the area of N14) also may account for the differences in S values.

The calculated infiltration rate (eq. 9) can be described numerically as the first derivative of cumulative infiltration compared to time (eq. 5). Infiltration rates near N85 and N14 were at or near steady-state within 1 to 2 hours after the start of ponding (figs. 5 and 6), although the model curve continued downward. The downward trend of the model curve is an artifact of using the Philip two-term equation rather than an expanded infinite-series solution of the equa-

Table 4. Calculated hydrologic parameters using the Philip two-term equation and corresponding experimentally extrapolated saturated hydraulic conductivity values

[All S (sorptivity) measurements in centimeters per square root of hours; all A and K_s (saturated hydraulic conductivity) measurements in centimeters per hour]

Location	Philip-equation parameters		
	S	A	K_s
UE-25 UZN #85, Ring 1	3.73	0.98	1.78
Ring 2	4.65	0.40	1.37
UE-25 UZN #14	9.40	12.94	17.79

tion (Swartzendruber and Clague, 1989, p. 621). This is not a considerable artifact because A is 0.3 to 0.6 times the value of K_s and is not used to any great extent for further analysis.

Although the S near N14 is more than twice as large as that at N85 (table 4), the differences are largely due to differences in θ_i, because, as θ_i approaches saturation, $S(\theta)$ approaches 0 (Chong and Green, 1979, p. 92–93; Chong and others, 1982, p. 229). By estimating S as a linear function of θ, infiltration at different locations that have differing θ_i can be compared. To compare the different soils at different θ, θ can be scaled as $\Theta = \theta/\theta_s$, where θ_s is water content at saturation and Θ is dimensionless soil-water content. The sorptivity-dimensionless soil-water characteristic curve is constructed as a linear function with $S = 0$ at $\Theta = 1$, crossing the measured point Θ_i, the initial dimensionless water content, and extrapolating or interpolating for different values of Θ_i. Initial soil-water contents were 0.15 cm^3/cm^3 (Θ = 0.58) at N85 and 0.03 cm^3/cm^3 (Θ = 0.07) at N14. The larger initial soil-water contents at the N85 location could account for much of the S differences between the two borehole locations. Further infiltration measurements made with differing θ_i are needed to determine if $S(\theta)$ for the unconsolidated materials covering Yucca Mountain has a linear relation.

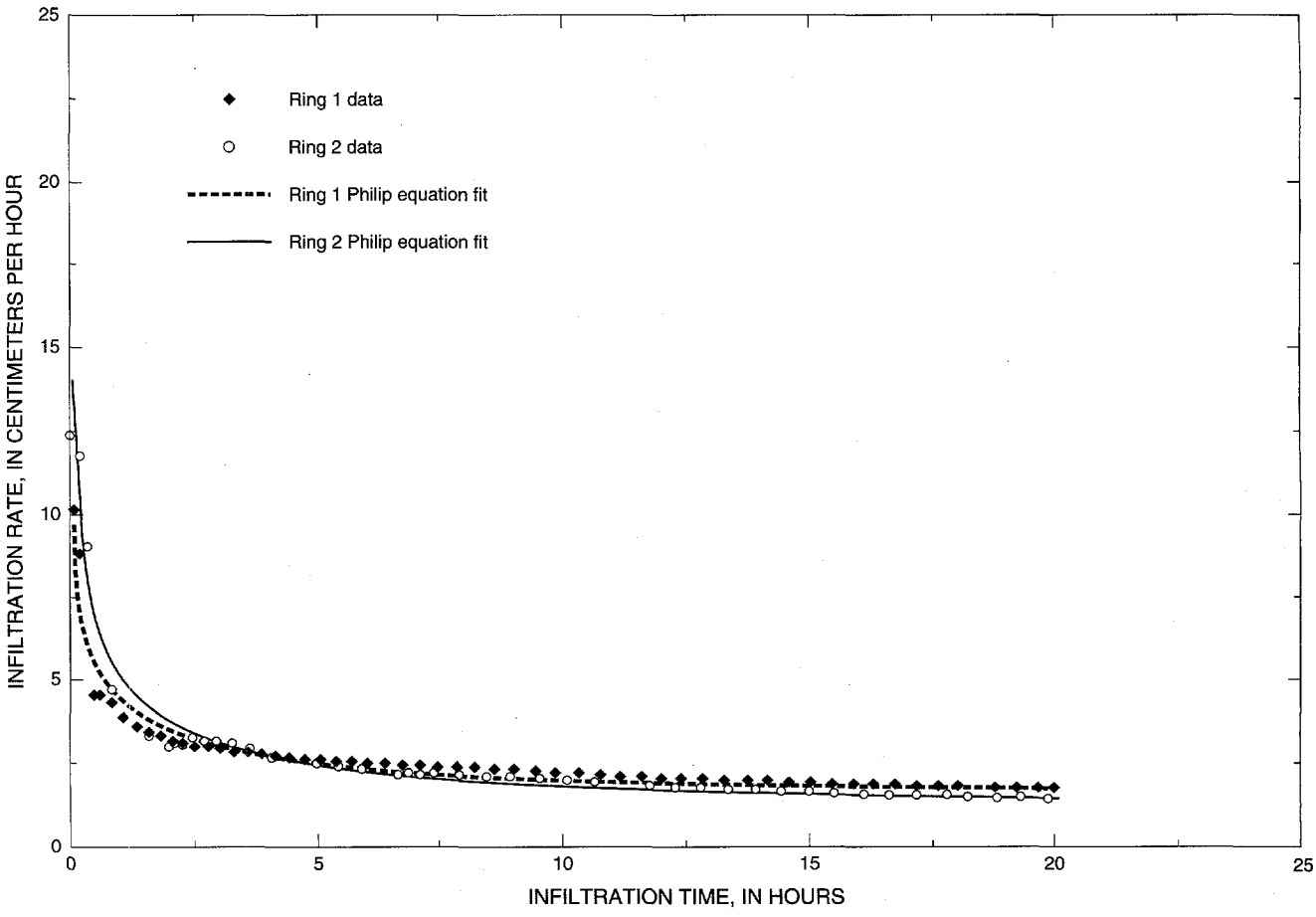

Figure 5. Infiltration-rate data and Philip-equation first derivative fit obtained near borehole UE-25 UZN #85, Yucca Mountain, Nevada.

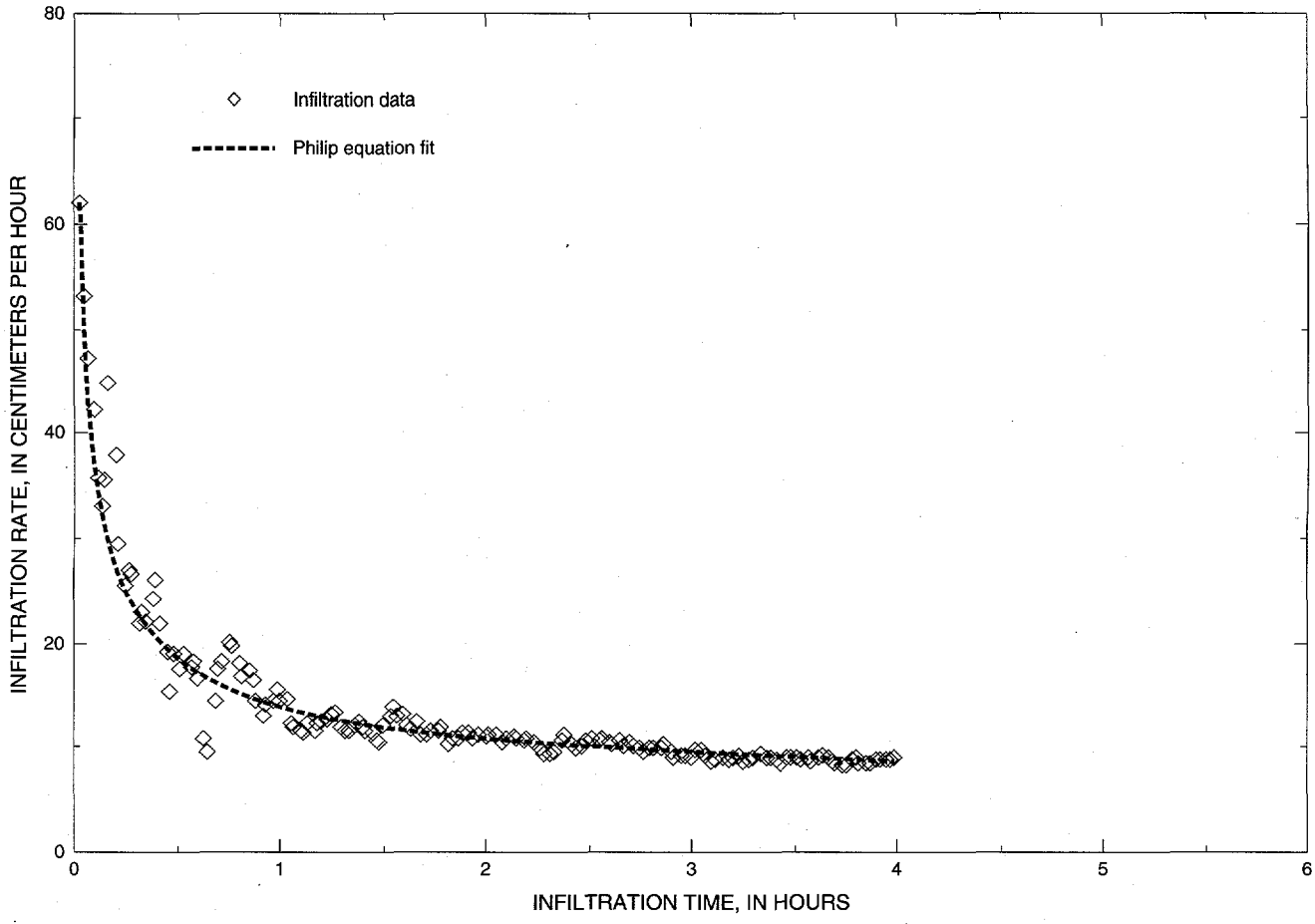

Figure 6. Infiltration-rate data and Philip-equation first derivative fit obtained near borehole UE-25 UZN #14, Yucca Mountain, Nevada.

SUMMARY

Hydrologic properties of the unconsolidated surficial materials covering Yucca Mountain are needed for interpretation of hydrologic data in the unsaturated zone and for input to hydrologic models. Two hydrologic properties, K_s and S, were derived from cumulative-infiltration and infiltration-rate measurements of the unconsolidated materials. The Philip equation, which numerically describes the infiltration process, was used to calculate K_s and S using the infiltration measurements.

Infiltrometers designed to measure cumulative infiltration and infiltration rates were evaluated for their applicability and practicality for measuring K_s and S of Yucca Mountain unconsolidated materials. Because of the skeletal nature of the unconsolidated materials, the tension infiltrometer, sprinkler-imposed steady-flux infiltrometer, and ring infiltrometer were determined to be the best suited infiltrometers for measuring infiltration on Yucca Mountain. To obtain an understanding of the range in K_s and S at Yucca Mountain, an immediate priority was set to develop and test a fairly simple ring infiltrometer.

A prototype automated ring infiltrometer was developed to obtain reliable cumulative-infiltration and infiltration-rate data. Cumulative-infiltration and infiltration-rate curves were obtained at two borehole locations on Yucca Mountain. The infiltration experiments were conducted over time periods ranging from 4 to 20 hours, which was adequate to obtain a steady-state infiltration rate from which K_s was extrapolated. Saturated hydraulic conductivity measurements differed by an order of magnitude between the two experiment sites.

The Philip two-term equation was used to calculate S and the A parameter related to K_s. Sorptivity measurements differed by more than 100 percent between the two experiment sites. The differences in S could be attributed mainly to differences in initial soil-

water contents at the experiment sites. Measured K_s values were within theoretical constraints of the calculated Philip A parameter. A qualitative comparison between K_s and S, and differences in measured physical characteristics of the surface materials, also helped explain infiltration differences between the two experiment sites. More infiltrometer measurements obtained at different initial soil-water contents and more detailed correlation studies between measured and derived hydrologic and physical properties of surface materials are needed to help understand infiltration capacities and variability on Yucca Mountain. The experiments helped define the methods needed to define selected hydrologic properties at Yucca Mountain.

REFERENCES CITED

Amoozegar, A., and Warrick, A.W., 1986, Hydraulic conductivity of saturated soils: Field methods, *in* Klute, A., ed., Methods of soil analysis—Physical and mineralogical methods, Part 1, (2d ed.): Madison, Wis., American Society of Agronomy, Agronomy 9, p. 735–768.

Bouwer, Herman, 1966, Rapid field measurement of air entry value and hydraulic conductivity of soil as significant parameters in flow system analysis: Water Resources Research, v. 2, no. 4, p. 729–738.

Bouwer, Herman, 1986, Intake rate—Cylinder infiltrometer, *in* Klute, A., ed., Methods of soil analysis—Physical and mineralogical methods, Part 1, (2d ed.): Madison, Wis., American Society of Agronomy, Agronomy 9, p. 825–844.

Chong, S.K., and Green, R.E., 1979, Application of field-measured sorptivity for simplified infiltration prediction, *in* Proceedings of the symposium on hydrologic transport modeling—New Orleans, La., 1979: American Society of Agricultural Engineers Publication 4–80, p. 88–96.

Chong, S.K., Green, R.E., and Ahuja, L.R., 1982, Determination of sorptivity based on in-situ soil water redistribution measurements: Soil Science Society of America Journal, v. 46, no. 2, p. 228–230.

Clothier, B.E., and White, I., 1981, Measurement of sorptivity and soil water diffusivity in the field: Soil Science Society of America Journal, v. 45, no. 2, p. 241–245.

Elrick, D.E., and Reynolds, D.W., 1993, Measurement of saturated and near-saturated soil hydraulic conductivity, *in* Topp, G.C., Reynolds, W.D., and Green, R.E., eds., Advances in measurement of soil physical properties—Bringing theory into practice: Madison, Wis., Soil Science Society of America, Special Publication 30, p. 1–24.

Flint, A.L., Flint, L.E., and Richards, K.A., 1994, Evaluation of measurement scale using imbibition experiments in volcanic tuffs: Soil Science Society of America Journal, v. 58, no. 1, p. 94–102.

Green, R.E., Ahuja, L.R., and Chong, S.K., 1986, Hydraulic conductivity, diffusivity, and sorptivity of unsaturated soils—Field methods, *in* Klute, A., ed., Methods of soil analysis—Physical and mineralogical methods, Part 1, (2d ed.): Madison, Wis., American Society of Agronomy, Agronomy 9, p. 771–798.

Hillel, Daniel, 1980, Applications of soil physics: New York, Academic Press, p. 5.

Hofmann, L.L., Guertal, W.G., Davies, W.J., and Flint, A.L., 1993, A large-scale, automated, constant-head, double-ring infiltrometer [abs.], *in* Agronomy Abstracts: Annual Meetings of the American Society of Agronomy, Crop Science Society of America, and Soil Science Society of America, November 7–12, Cincinnati, Ohio, 1993, p. 208.

Koorevaar, P., Menelik, G., and Dirksen, C., 1983, Elements of soil physics: New York, Elsevier, 228 p.

Logsdon, S.D., and Jaynes, D.B., 1993, Methodology for determining hydraulic conductivity with tension infiltrometers: Soil Science Society of America Journal, v. 57, no. 6, p. 1426–1431.

Perroux, K.M., and White, I., 1988, Designs of disc permeameters: Soil Science Society of America Journal, v. 52, no. 5, p. 1205–1215.

Philip, J.R., 1957, The theory of infiltration—4. Sorptivity and algebraic infiltration equations: Soil Science, v. 84, p. 257–264.

Schmidt, M.R., Kolm, K.E., and Flint, A.L., 1992, Classification of upland soils by physical properties affecting infiltration in southern Nevada using the genesis-lithology-qualifier mapping system: Bulletin of the Association of Engineering Geologists, v. 29, no. 1, p. 33–47.

Scott, R.B., and Castellanos, M., 1984, Stratigraphic and structural relations of volcanic rocks in drill holes USW GU-3 and USW G-3, Yucca Mountain, Nye County, Nevada: U.S. Geological Survey Open-File Report 84–0491, p. 7–12.

Sharma, M.L., Gander, G.A., and Hunt, C.G., 1980, Spatial variability of infiltration in a watershed: Journal of Hydrology, v. 45, no. 1–2, p. 101–122.

Swartzendruber, D., and Youngs, E.G., 1974, A comparison of physically-based infiltration equations: Soil Science, v. 117, p. 165–167.

Swartzendruber, D., and Clague, F.R., 1989, An inclusive infiltration equation for downward water entry into soil: Water Resources Research, v. 25, no. 4, p. 619–626.

Talsma, T., 1969, In-situ measurement of sorptivity: Australian Journal of Soil Research, v. 7, p. 269–276.

Talsma, T., and Parlange, J.-Y., 1972, One-dimensional vertical infiltration: Australian Journal of Soil Research, v. 10, no. 2, p. 143–150.

U.S. Soil Conservation Service, 1975, Family and series differentiae and names, *in* Soil taxonomy—A basic system of soil classification for making and interpreting soil surveys: U.S. Department of Agriculture, Handbook 436, p. 383–405.

White, I., and Perroux, K.M., 1987, Use of sorptivity to determine field soil hydraulic properties: Soil Science Society of America Journal, v. 51, no. 5, p. 1093–1101.

White, I., and Perroux, K.M., 1989, Estimation of unsaturated hydraulic conductivity from field sorptivity measurements: Soil Science Society of America Journal, v. 53, no. 2, p. 324–329.

Wittwer, C.S., Bodvarsson, G.S., Chornack, M.P., Flint, A.L., Flint, L.E., Lewis, B.D., Spengler, R.W., and Rautman, C.A., 1992, Design of a three-dimensional site-scale model for the unsaturated zone at Yucca Mountain, Nevada, *in* High Level Radioactive Waste Management Conference; Proceedings of the third International conference: La Grange Park, Ill., American Nuclear Society, Inc., and American Society of Civil Engineers, p. 263–271.

Youngs, E.G., 1968, An estimation of sorptivity for infiltration studies from moisture moment considerations: Soil Science, v. 106, no. 3, p. 157–163.

Zimmerman, R.W., and Bodvarsson, G.S., 1989, An approximate solution for one-dimensional absorption in unsaturated porous media: Water Resources Research, v. 25, no. 6, p. 1422–1428.

☆ U.S. GOVERNMENT PRINTING OFFICE: 2000 — 673-082 / 47035 Region No. 8